Optimal Synchronization of a Memristive Chaotic Circuit

5 authors, including:

Michaux Kountchou Noube
Institute of Geological and Mining Research
9 PUBLICATIONS **17** CITATIONS

SEE PROFILE

Patrick Louodop
Université de Dschang
21 PUBLICATIONS **68** CITATIONS

SEE PROFILE

Fotsin Hilaire
61 PUBLICATIONS **524** CITATIONS

SEE PROFILE

Some of the authors of this publication are also working on these related projects:

Project Neuronal system View project

Optimal Synchronization of a Memristive Chaotic Circuit

Michaux Kountchou* and Patrick Louodop†
Laboratory of Electronics and Signal Processing,
Department of Physics, Faculty of Science,
University of Dschang, P. O. Box 67 Dschang, Cameroon
*kountchounoube@yahoo.fr
†louodop@yahoo.fr

Samuel Bowong‡
Laboratory of Applied Mathematics,
Department of Mathematics and Computer Science,
Faculty of Science, University of Douala,
P. O. Box 24157 Douala, Cameroon
sbowong@gmail.com

Hilaire Fotsin
Laboratory of Electronics and Signal Processing,
Department of Physics, Faculty of Science,
University of Dschang, P. O. Box 67 Dschang, Cameroon
hbfotsin@yahoo.fr

Jurgen Kurths§
Potsdam Institute for Climate Impact Research (PIK),
Telegraphenberg A 31, 14412 Potsdam, Germany
Jurgen.Kurths@pik-potsdam.de

This paper deals with the problem of optimal synchronization of two identical memristive chaotic systems. We first study some basic dynamical properties and behaviors of a memristor oscillator with a simple topology. An electronic circuit (analog simulator) is proposed to investigate the dynamical behavior of the system. An optimal synchronization strategy based on the controllability functions method with a mixed cost functional is investigated. A finite horizon is explicitly computed such that the chaos synchronization is achieved at an established time. Numerical simulations are presented to verify the effectiveness of the proposed synchronization strategy. Pspice analog circuit implementation of the complete master-slave-controller systems is also presented to show the feasibility of the proposed scheme.

Keywords: Memristor; memristive devices; chaotic circuit; optimal synchronization; Pspice analog circuit implementation.

*Nuclear Technology Section, Institute of Geological and Mining Research, P. O. Box 4110 Yaounde, Cameroon.

†Instituto de Física Teórica, UNESP, Universidade Estadual Paulista, Rua Dr. Bento Teobaldo Ferraz 271, Bloco II, Barra Funda, 01140-070 São Paulo, Brazil.

‡UMI 209 IRD & UPMC UMMISCO, Bondy, France, LIRIMA, project team GRIMCAPE, Yaounde, Cameroon, The African Center of Excellence in Information and Communication, Technologies (CETIC), University of Yaounde 1, Cameroon.

‡Author for correspondence

§Department of Physics, Humboldt Universitat zu Berlin, 12489 Berlin, Germany.

1. Introduction

Since its recent invention, the memristor has proven to be a revolutionary device due to the versatility of its applications. High scale of integration, memory functions and some other attractive characteristics make the memristor one of the most revolutionary device since the invention of the transistor. Thus, after the realization of a solid-state thin film two terminal memristor [Strukov *et al.*, 2008], a considerable number of potential memristor-based applications have been reported like high-speed low-power processors [Yang *et al.*, 2013], adaptive filter [Driscoll *et al.*, 2010], pattern recognition systems [Corinto *et al.*, 2012], associative memory [Pershin & Ventra, 2010], neural networks [Adhikari *et al.*, 2012; Ascoli & Corinto, 2013; Wen *et al.*, 2015; Zhao *et al.*, 2015], programmable analog integrated circuits [Shin *et al.*, 2011], and so on [Ascoli *et al.*, 2013; Tetzlaff, 2014]. Interestingly, the intrinsic nonlinear characteristic of memristors has been exploited in implementing novel chaotic oscillators with complex dynamics [Itoh & Chua, 2008; Muthuswamy, 2010; Muthuswamy & Chua, 2010; Lu *et al.*, 2015]. However, the design of the circuit, in which the properties of these memristors characterized by numerous nonlinearities are used, requires extensive simulations and experimental verifications. Thus, an equivalent circuit model is desirable to realize a memristor. Such a model must take into account the physical properties of the memristor which lead to its nonlinear and hysteretic behaviors. Several approaches have been already presented: mutators for which current-controlled voltage sources and voltage-controlled current sources involving several operational amplifiers and transistors are needed [Chua, 1971], microcontrollers [Pershin & Ventra, 2010], and analog multipliers [Muthuswamy, 2010], implementing memristors with a cubic characteristic, generalized memristor consisting of diode bridge [Bao *et al.*, 2014; Lu *et al.*, 2015].

Chaotic behavior may be unpredictable, uncoordinated, and constantly shifting under many circumstances. Because of this, chaotic dynamics and chaos synchronization are always some hot research fields. The interest in synchronization lies on the potential applications in areas such as biological oscillators, animal gaits, and secure communication. Since the seminal work of [Pecora & Carroll, 1990], chaos synchronization has been investigated leading to various types of synchronization such as complete synchronization [Mahmoud & Mahmoud, 2010], phase synchronization [Junge & Parlitz, 2000], lag synchronization [Shahverdiev *et al.*, 2002], generalized synchronization [Wang & Guan, 2006], projective synchronization [Li, 2012] and combination synchronization. According to the various types of synchronization, several techniques such as variable structure control [Yin *et al.*, 2002], active control [Ho & Hung, 2002], impulsive control [Itoh *et al.*, 2001], fuzzy control [Wang, 1993], adaptive control [Fotsin & Daafouz, 2005], sliding mode control [Li *et al.*, 2012], nonlinear feedback control [Effa *et al.*, 2009], time-delay feedback control [Louodop *et al.*, 2014a], and the backstepping control [Bowong, 2004] are developed. The techniques used generally lead to acceptable performance.

Nevertheless, these methods have generally a drawback, because their physical implementation would appear to be a very hard task. Furthermore, the most common studies' approaches are numerical simulations associated to the well-known analytical perturbation methods. However, it is well known that with such techniques appear problems related to time integration. Indeed, even with very fast workstations, scanning parameter spaces turns out to be a very slow process. Moreover, to the best of author's knowledge, there exists no method that can help to predict the duration of the transient phase of a numerical simulation. The analog simulation offers the way to tackle such difficulties. This is one of the major reasons for the increasing interest devoted to this type of simulation for the analysis of nonlinear and chaotic physical systems [Kountchou *et al.*, 2014; Louodop *et al.*, 2014b]. Indeed, a properly designed circuit can provide sufficiently good real-time results faster than a numerical simulation on a fast computer. Moreover, analog computation reveals itself to be very powerful for a large number of specific problems such as pattern recognition and image processing just to name a few.

Motivated by complex dynamical behaviors of chaotic systems and noticeable characteristics of memristors, a memristor based chaotic system is proposed. The dynamical behaviors of the proposed memritive system are investigated. We propose an appropriate electronic circuit (analog simulator) to investigate the dynamical behavior of the system. Correspondences are established between the coefficients of the model system and the components of the electronic circuit. A comparison of Pspice and numerical results shows a very good agreement.

Next, we use the controllability functions method to propose an optimal robust feedback coupling which accomplishes the synchronization between two chaotic memristive systems at a finite time. The expression of the synchronization time is explicitly computed. We refer the reader to [Korobov *et al.*, 1993] for more informations about the controllability functions method. The advantage of the proposed scheme is that it takes into account the energy wasted by the feedback coupling and the closed-loop performance on synchronization. The robustness of the feedback coupling against model uncertainties is shown through numerical and Pspice simulations.

The rest of the manuscript is organized as follows. Section 2 introduces the mathematical model and deals with the dynamics of the proposed memristive system. The dynamical behavior of the system is also investigated through an appropriate electronic circuit. In Sec. 3, we investigate the optimal robust synchronization between two chaotic memritive systems. Numerical and Pspice simulations are given to show the effectiveness and applicability of the proposed synchronization method. The concluding remarks are given in Sec. 4.

2. The Circuit and Its Dynamics

2.1. *The circuit*

Chua and Kang [1976] introduced a memristive system by generalizing the original definition of a memristor. A memristive system is generally described by

$$
\begin{cases}
\dot{x}_3 = F(x_3, x_2, t), \\
y = G(x_3, x_2, t)x_2,
\end{cases} \tag{1}
$$

where x_2, y and x_3 denote the input, output, and state of the memristive system, respectively. The function F is a continuous n-dimensional vector function and G a continuous scalar function. Based on the definition of memristive system (1), we propose a memristive device in the following form:

$$
\begin{cases}
\dot{x}_3 = -p_2 x_2, \\
y = (1 + x_3^2 - x_3^4)x_2,
\end{cases} \tag{2}
$$

where G given in memristive system (1) is a fourth degree polynomial function and p_2 a positive constant. In order to investigate the fingerprints of memristive device (2), an external bipolar period signal is applied across its terminals. The external

sinusoidal stimulus is given by

$$
x_2 = U\sin(2\pi ft), \tag{3}
$$

where U and f are respectively, the amplitude and frequency.

Figure 1(a) shows the hysteresis loop of the memristive device (2) driven by a periodic signal (3) with different frequencies. Obviously, the proposed memristive device exhibits a "pinched hysteresis loop" in the input–output plane, namely there may be at most two values of the output y for a given input x_2. In addition, when the excitation frequency increases, the hysteresis lobe area decreases monotonically. Moreover, when the frequency is adequately large, the pinched hysteresis loop shrinks to a single-valued function. It is worth noting that the hysteresis loop of the memristive device (2) is pinched at different input amplitudes [see Fig. 1(b)]. Additionally, the output y also depends on the initial state of the memristive device, as depicted in Fig. 1(c). Thus, according to [Adhikari *et al.*, 2013] the three main fingerprints of memristive system have been observed in the proposed memristive device (2).

In this paper, we suppose that the internal state variable x_3 of the memristive device (2) is accessible for designing the other state variables as presented in the sequel. Then, based on the memristive device (2), a three-dimensional autonomous memristive system is proposed as follows:

$$
\begin{cases}
\dot{x}_1 = x_3 + p_1 y, \\
\dot{x}_2 = x_1 - x_2 + x_3, \\
\dot{x}_3 = -p_2 x_2,
\end{cases} \tag{4}
$$

where p_1 and p_2 are positive real parameters, $y = (1 + x_3^2 - x_3^4)x_2$ is the output of the memristive system. Here, the internal state variable of the memristor is represented by the third equation of system (4), while the output y of the memristor is introduced in the first equation of system (4). Note that the state variable x_3 of the memristor is introduced in the first and second equations of system (4) because, as we explained before, this internal state x_3 is accessible for designing the two other state variables x_1 and x_2.

Nevertheless, it is also possible to obtain a system that operates correctly, even if the internal state variable x_3 of the memristor is not accessible. To obtain this system, one must merely replace the state variable x_3 which is introduced in the first
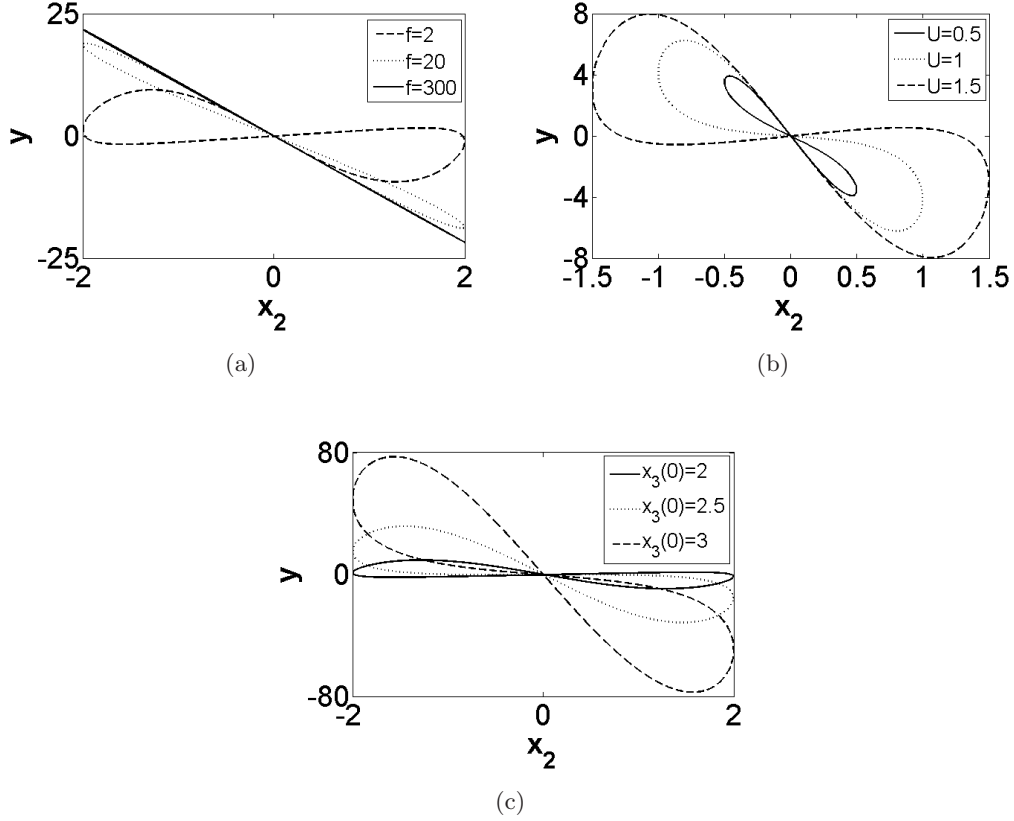
(a)

(b)

(c)

Fig. 1.   Hysteresis loops of the memristive device (2) driven by a sinusoidal stimulus Eq. (3) when (a) $U = 2$, $x_3(0) = 2$, and varying frequency f, (b) $f = 2$, $x_3(0) = 2$, and changing input amplitude U, and (c) $U = 2$, $f = 2$, and using different initial states $x_3(0)$ ($p_2 = 4$).

and second equations of system (4) by the external stimulus voltage $v = \cos(wt)$. Thus, we obtain the following nonautonomous memristive system:

$$\begin{cases} \dot{x}_1 = v + p_1 y, \\ \dot{x}_2 = x_1 - x_2 + v, \\ \dot{x}_3 = -p_2 x_2. \end{cases} \qquad (5)$$

The synoptic diagram of memristive systems (4) and (5) is depicted in Fig. 2. On this diagram, the bidirectional switch permits to select the operation of one or the other of these two systems independently. In the sequel, we will show that, these two systems can generate the chaotic dynamical behaviors for the suitable selected parameters. To do so, without loss of generality, we will focus our work on the first autonomous system (4).

It is easy to see that, the intrinsic nonlinear characteristic of memristor has been exploited for implementing novel chaotic oscillators with complex dynamics. The motivation of such study comes to the fact that the analysis and physical implementation of the proposed memristive system (4) are

particularly straightforward. Also, this system (4) is an appropriate candidate for applications in engineering such as random bit generation, secure communications as well as sonar and radar systems.
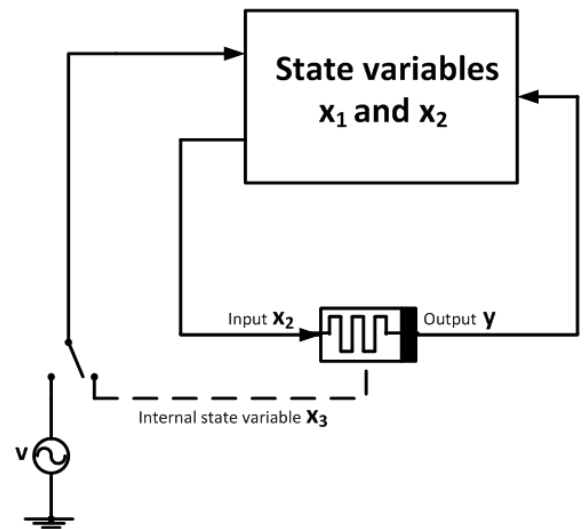

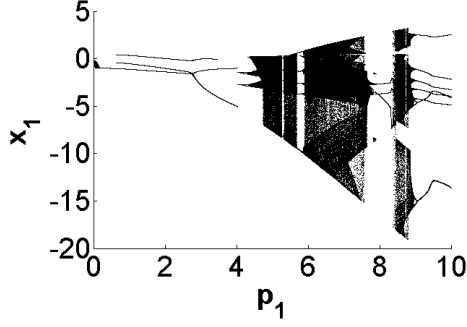Fig. 2.   The synoptic diagram of the proposed memristive systems (4) and (5).

Fig. 3. Bifurcation diagram by varying parameter p_1 in $[0, 10]$.

2.2. Basic dynamics analysis

Herein, we analyze some basic dynamics of the memristive system (4), including dissipation characteristic, stability of equilibria and the bifurcation diagram analysis when the parameter p_1 varies.

2.2.1. Symmetry, dissipation, stability of equilibria and chaotic behavior
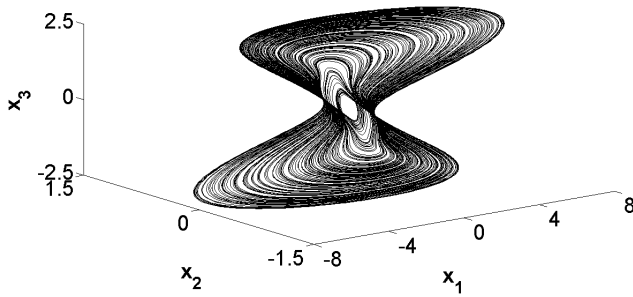
For variable substitution of the system: $(x_1, x_2, x_3) \rightarrow (-x_1, -x_2, -x_3)$, its type form is still the same, it is easy to show that system (4) is symmetrical about the original point. To ensure that system (4) is chaotic, we consider the general condition of dissipativity which gives
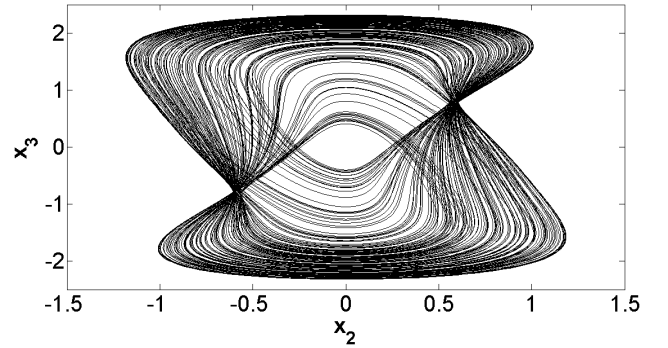
$$\nabla V = \frac{\partial \dot{x}_1}{\partial x_1} + \frac{\partial \dot{x}_2}{\partial x_2} + \frac{\partial \dot{x}_3}{\partial x_3} = -1. \quad (6)$$

System (4) is dissipative, and due to the index form: $dV/dt = e^{-t}$, it converges to the volume element V_0 at time t, so its form of convergence for the volume element is $V_0 e^{-t}$, which means that all system trajectories will be limited to the point of zero volume set, its behavior will be fixed in the attractor when $t \rightarrow \infty$.
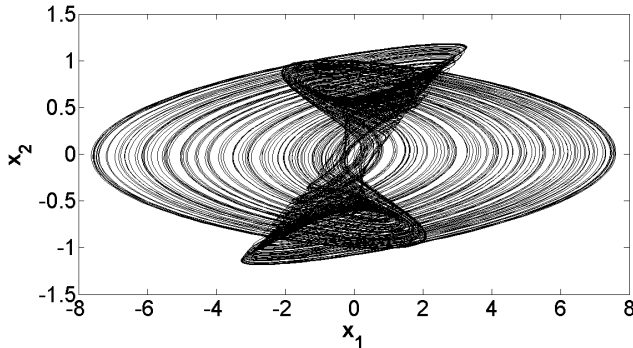
Equilibria of the memristive system are obtained by setting to zero the right-hand side of system (4). System (4) has a single equilibrium point $E_0 = (0, 0, 0)^\top$. Note that, the values of the parameters p_1 and p_2 are chosen to be $p_1 = 5$ and $p_2 = 4$. Then, the eigenvalues associated to E_0 are $\lambda_1 = -2.2419$, $\lambda_2 = 0.62094 - 1.1827i$ and $\lambda_3 = 0.62094 + 1.1827i$. Since λ_1 is a negative real number, λ_2 and λ_3 are a pair of complex conjugate eigenvalues with positive real parts, the equilibrium point E_0, is an unstable saddle point.
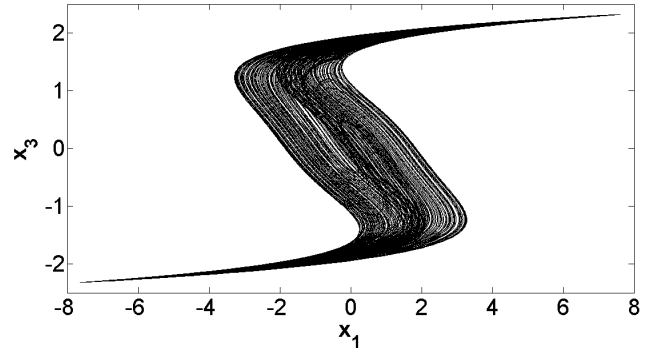

(a)

(b)

(c)

(d)

Fig. 4. Phase portraits of the memristive system (4) when $p_1 = 5$ and $p_2 = 4$.
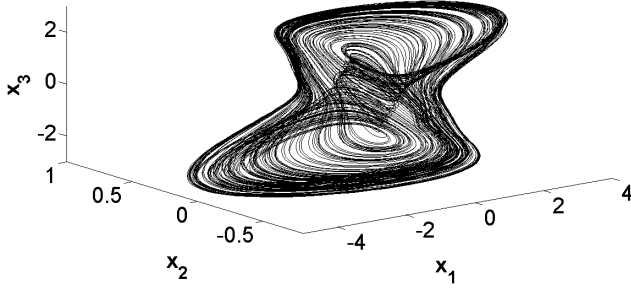
Fig. 5.   Phase portraits of the memristive system (5) when $p_1 = 2$, $p_2 = 6$ and $w = 2.5$.

Now, we set $p_2 = 4$ and p_1 varies. Thus, system (4) can generate chaotic dynamical behaviors in a wide region as shown in Fig. 3, which presents the bifurcation diagram. This figure clearly shows a very rich and striking dynamic behavior when the parameter p_1 is varied. The chaotic phase portraits are depicted in Fig. 4 when $p_1 = 5$ and $p_2 = 4$. Note that system (5) can also generate chaotic dynamical behaviors for the following set of parameters: $p_1 = 2$, $p_2 = 6$ and $w = 2.5$ (see Fig. 5).

2.3. *Analog circuit implementation of the memristive chaotic system*

Herein, a circuit realization of system (4) is investigated to illustrate the feasibility and correctness of the theoretical model. The designed electronic circuit is shown in Fig. 6 where the variables x_1, x_2, x_3 of system (4) are the voltages across the capacitors C_{x_1}, C_{x_2} and C_{x_3} respectively. As shown in Fig. 6, the main component of the circuit is the memristive device, which is realized by common electronic components as presented in the red box. Hence, the proposed memristive device is characterized by the following circuital equations (see Fig. 7):

$$\begin{cases} \dot{x}_3 = -\dfrac{1}{10^4 R_{p_2} C_{x_3}} x_2, \\ y = (V_1 + x_3^2 - x_3^4) x_2. \end{cases} \qquad (7)$$

By using Kirchhoff's circuit laws, the equations of the circuit in Fig. 6 are derived as follows:

$$\begin{cases} \dot{x}_1 = x_3 + \dfrac{1}{10^4 R_{p_1} C_{x_1}} y, \\ \dot{x}_2 = x_1 - x_2 + x_3, \\ \dot{x}_3 = -\dfrac{1}{10^4 R_{p_2} C_{x_3}} x_2, \end{cases} \qquad (8)$$

where

$$p_1 = \frac{1}{10^4 R_{p_1} C_{x_1}}, \quad p_2 = \frac{1}{10^4 R_{p_2} C_{x_3}} \quad \text{and} \quad V_1 = 1.$$

The time unit is 10^{-4} sec. It is worth mentioning that the time scaling process offers to the analog
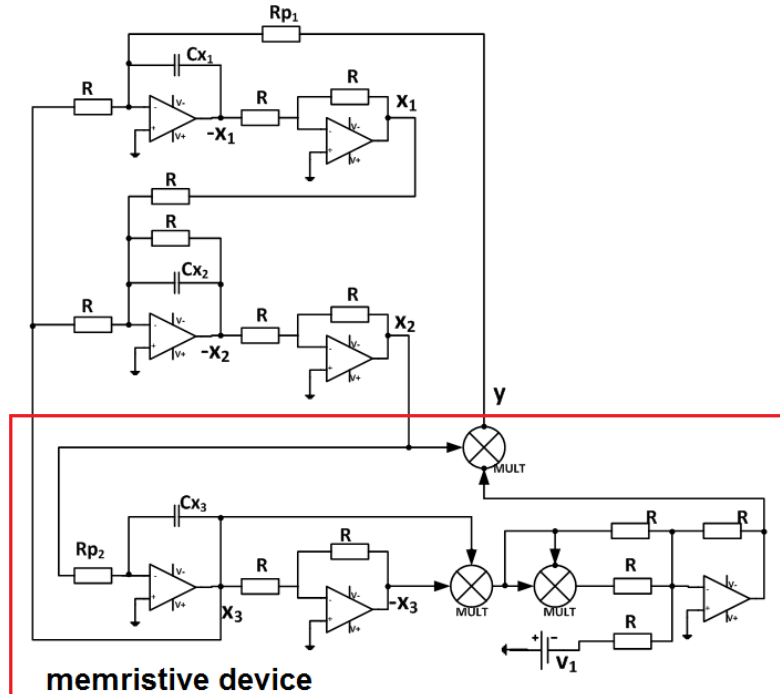

Fig. 6.   Schematic of the circuital implementation of the memristive system (4).
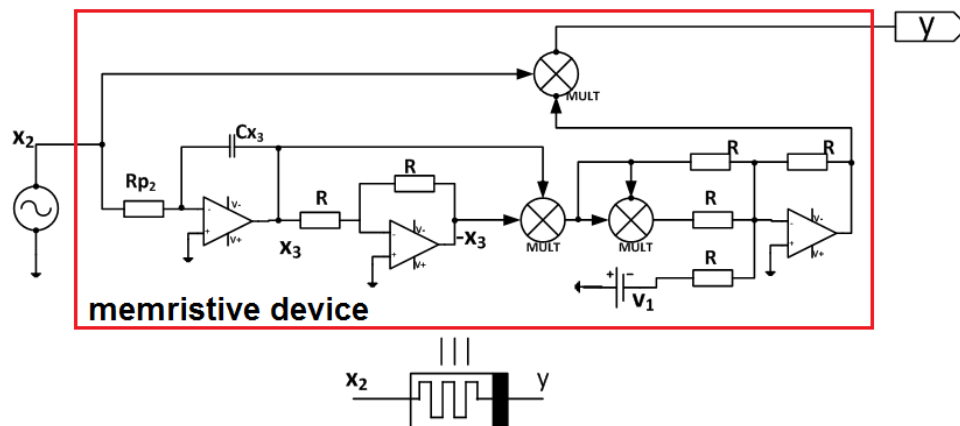
Fig. 7.   Circuitry implementation of the memristive device (2) driven by a sinusoidal stimulus.
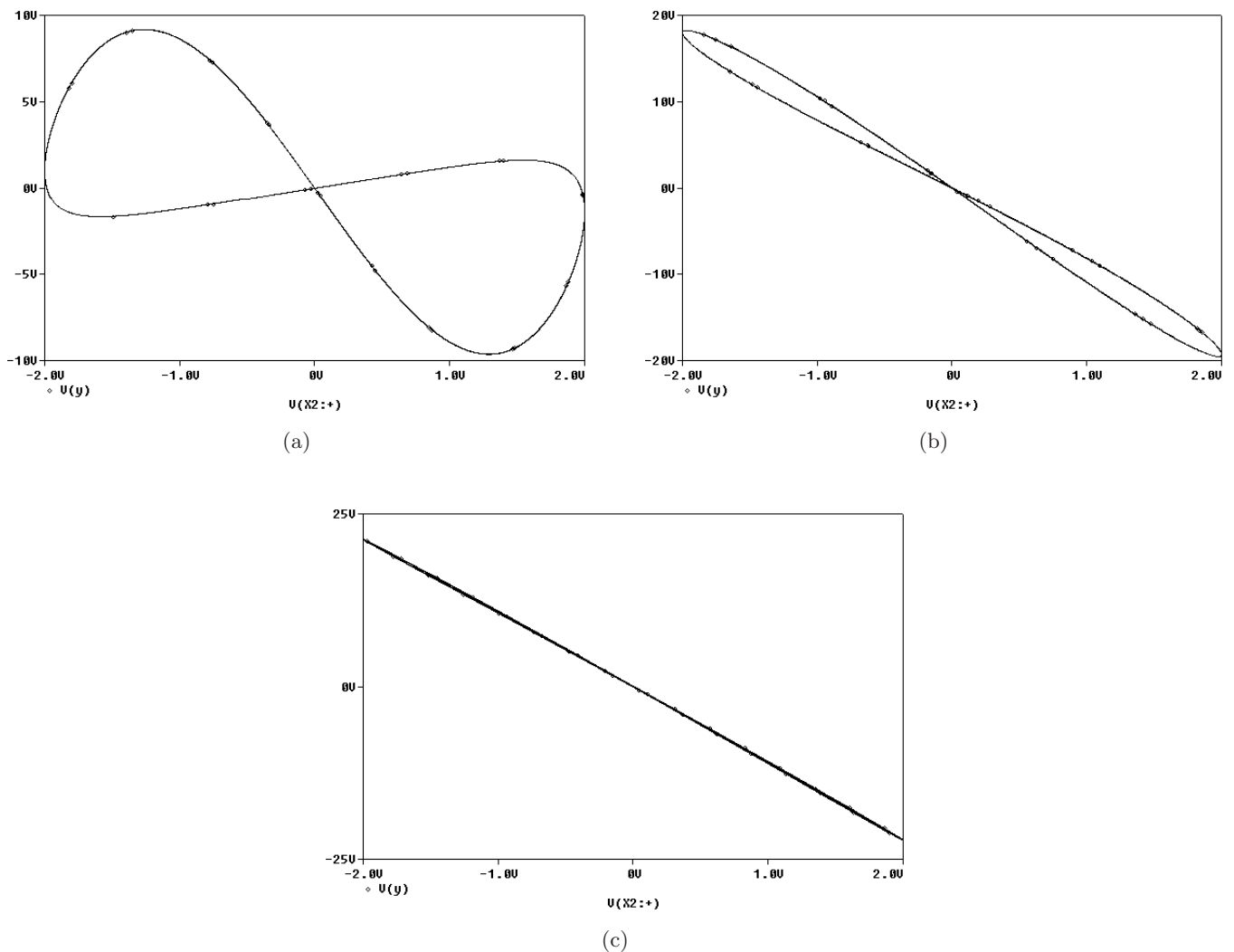

(a)

(b)

(c)

Fig. 8.   Pspice simulation of the pinched hysteresis loops of the memristive device (2) driven by a sinusoidal stimulus under amplitude 2 V and varying frequency $f = 20\,\text{kHz}$, $f = 200\,\text{kHz}$, $f = 3000\,\text{kHz}$ with initial condition $V_{C_{x_3}}(0) = -2$.

devices the possibility to operate under their bandwidth. The time scaling process is also of high importance while performing analog computation. It offers the possibility to simulate the behavior of the system at any given frequency by performing an appropriate time scaling that consists of expressing the time variable T_M using numerical simulation in Matlab versus the Pspice computation time T_S:

$$T_S = RCT_M = 10^{-a}T_M. \tag{9}$$

Then,

$$f_S = \frac{1}{RC}f_M = 10^a f_M, \tag{10}$$

where a is a positive integer depending on the values of the resistors and capacitors used in the analog simulation. Here, $R = 10\,\text{k}\Omega$ and $C = 10\,\text{nF}$ so that $a = 4$.

The following values of circuits components are selected: $C_{x_1} = C_{x_2} = C_{x_3} = C = 10\,\text{nF}$, $R = 10\,\text{k}\Omega$, $R_{p_1} = 2\,\text{k}\Omega$, $R_{p_2} = 2.5\,\text{k}\Omega$ and $V_1 = 1\,\text{V}$. The voltage source is set at $\pm 15\,\text{Vdc}$. The choice of these values is justified by fact that we want to use the same sets of system parameters for both numerical and experimental studies. The Pspice simulation results of the input–output curves of the memristive device with a periodic input under amplitude $2\,\text{V}$ and varying frequency $f = 20\,\text{kHz}$, $f = 200\,\text{kHz}$ and $f = 3000\,\text{kHz}$ with the initial condition $V_{C_{x_3}}(0) = -2$ are depicted in Fig. 8, by using the analog circuit of Fig. 7. One can observe that, the numerical [Fig. 1(a)] and Pspice (Fig. 8) curves are consistent with each other. The Pspice simulation results for the proposed chaotic circuit are shown in Fig. 9. There clearly appears a good agreement between the theoretical attractor (Fig. 4) and the circuital one (Fig. 9).
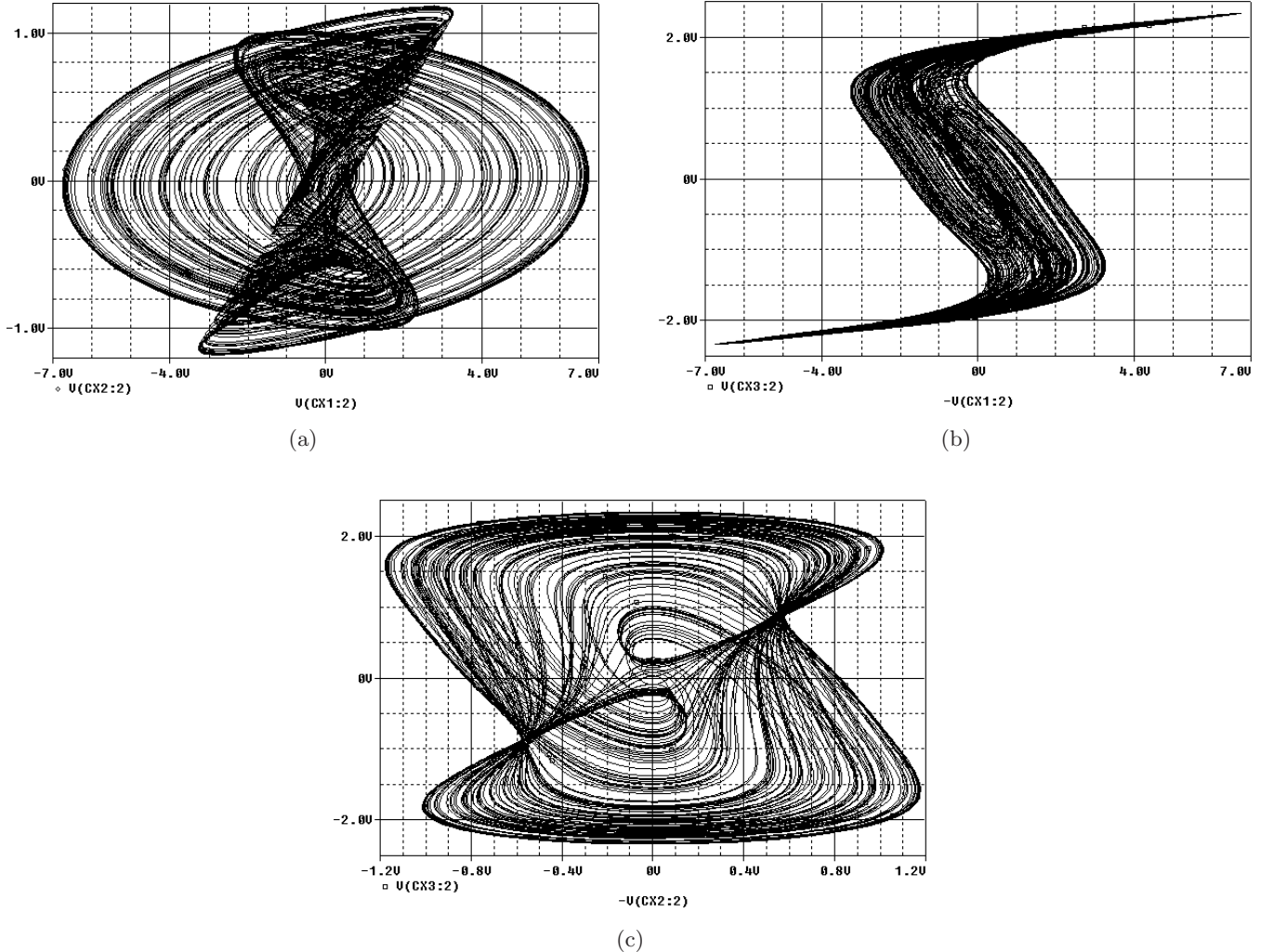

(a)

(b)

(c)

Fig. 9. Phase portrait using Pspice simulations of the memristive chaos generator when $R_{p_1} = 2\,\text{k}\Omega$ and $R_{p_2} = 2.5\,\text{k}\Omega$.

3. Optimal Synchronization

3.1. *Synchronization problem*

In this section, we state the synchronization problem. Let us consider the following chaotic system as the drive system:

$$\begin{cases} \dot{x}_1 = x_3 + p_1(1 + x_3^2 - x_3^4)x_2, \\ \dot{x}_2 = x_1 - x_2 + x_3, \\ \dot{x}_3 = -p_2x_2. \end{cases} \quad (11)$$

The slave system is constructed as follows:

$$\begin{cases} \dot{y}_1 = y_3 + p_1(1 + y_3^2 - y_3^4)y_2 + u, \\ \dot{y}_2 = y_1 - y_2 + y_3, \\ \dot{y}_3 = -p_2y_2, \end{cases} \quad (12)$$

where u is the feedback coupling.

The synchronization problem can be stated as follows: given the transmitted signal x_1 and least prior information about the structure of system (11), to design a feedback coupling u such that which synchronizes the orbits of both the drive and response systems at an established finite time T, i.e.

$$\lim_{t \to T} y_1(t) = x_1(t). \quad (13)$$

Now, let us define the synchronization error as follows:

$$e_i = y_i - x_i, \quad i = 1, 2, 3. \quad (14)$$

Then, the synchronization error dynamics is

$$\begin{cases} \dot{e}_1 = \Delta F + u, \\ \dot{e}_2 = e_1 - e_2 + e_3, \\ \dot{e}_3 = -p_2e_2, \end{cases} \quad (15)$$

where $\triangle F$ is a smooth vector field defined as follows:

$$\Delta F = e_3 + p_1(1 + (e_3 + x_3)^2 - (e_3 + x_3)^4)$$
$$\times (e_2 + x_2) - p_1(1 + x_3^2 - x_3^4)x_2.$$

In this way, the synchronization problem can be seen as the stabilization of Eq. (15) at the origin in a finite horizon. In other words, the problem is to find a robust feedback coupling u such that $\lim_{t \to T} \|e(t)\| \approx 0$ (which implies that $x_i(t) \approx y_i(t)$ for all $t \geq T > 0$, $i = 1, \dots, 3$).

Now, let $\zeta_1 = e_2$ and $\zeta_2 = e_3$. Then, system (15) can be changed into a canonical form [Bowong,

2004; Femat *et al.*, 1999; Gonzalez *et al.*, 1999] as follows:

$$\begin{cases} \dot{e}_1 = \Theta(e_1, \zeta, u) + u, \\ \dot{\zeta}_1 = e_1 - \zeta_1 + \zeta_2, \\ \dot{\zeta}_2 = -p_2\zeta_1, \\ y_e = e_1, \end{cases} \quad (16)$$

where y_e denotes the output of the error system, $\zeta \in \mathbb{R}^2$ is the unobservable state vector (internal dynamics). The function $\Theta(e_1, \zeta, u)$ is uncertain and defined as follows

$$\Theta(e_1, \zeta, u) = \zeta_2 + p_1(1 + (\zeta_2 + x_3)^2 - (\zeta_2 + x_3)^4)$$
$$\times (\zeta_1 + x_2) - p_1(1 + x_3^2 - x_3^4)x_2.$$

In the sequel, we assume that only the system output $y_e = e_1$ is available for feedback.

To deal with the uncertain term $\Theta(e_1, \zeta, u)$ in Eq. (16), we lump it into a new state. Thus, let $\eta = \Theta(e_1, \zeta, u)$. In this way, following [Bowong, 2004; Femat *et al.*, 1999; Gonzalez *et al.*, 1999] system (16) can be rewritten as the dynamically equivalent extended system

$$\begin{cases} \dot{e}_1 = \eta + u, \\ \dot{\eta} = \Gamma(e_1, \eta, \zeta, u, \dot{u}), \\ \dot{\zeta} = \Psi(e_1, \zeta), \end{cases} \quad (17)$$

where

$$\zeta = (\zeta_1, \zeta_2)^\top, \quad \Psi(e_1, \zeta) = (e_1 - \zeta_1 + \zeta_2, -p_2\zeta_1)^\top,$$
$$\Gamma(e_1, \eta, \zeta, u, \dot{u}) = \dot{\eta} = \dot{\Theta}.$$

At this stage, we point out that system (17) is minimum phase, that is, the zero dynamics $\dot{\zeta} = \Psi(0, \zeta)$ converges to the origin. In other words, the closed-loop system is internally stable. In order, to illustrate that system (17) satisfies the minimum phase property, one may prove that $\dot{\zeta}_1 = e_1 - \zeta_1 + \zeta_2$ and $\dot{\zeta}_2 = -p_2\zeta_1$ converge asymptotically to zero when $e_1 = 0$. Note that $\zeta = (\zeta_1, \zeta_2)^\top$ is bounded. Thus, the zero dynamics can be written as

$$\dot{\zeta} = E\zeta,$$

where

$$E = \begin{bmatrix} -1 & 1 \\ -p_2 & 0 \end{bmatrix},$$

which is Hurwitz because $p_2 > 0$. Then, the zero dynamics subsystem $\dot{\zeta} = E\zeta + H$ is asymptotically stable. Hence, system (17) is minimum

phase. Then, when we have taken actions to achieve $\lim_{t \to T} e_1(t) = 0$, the part $\Psi(e_1, \zeta) \to \Psi(0, \zeta) \to 0$ as $t \to \infty$ asymptotically for the so-called minimum-phase character.

3.2. *Design of the feedback coupling*

Herein, the problem of designing the feedback coupling u is addressed in such a manner that energy wasted by the feedback is accounted. The approach developed considers incomplete state measurements and no detailed model of the systems to guarantee robust stability (in fact, robust synchronization). This approach includes an uncertainty estimator and leads to a robust adaptive feedback control scheme. Towards the optimization problem, the first step in our approach is to consider the transitive of states. To this end, the following mixed cost function is defined by quantifying the transient trajectory of the synchronization error [Korobov *et al.*, 1993]:

$$J(u) = k^2 T + \int_{t_0}^{T} [(We_1, e_1) + (Uu, u)]dt,$$
$$k > 0, \quad (18)$$

where k is a constant gain, $t_0 \geq 0$ is the time at which the synchronization process starts and $T > t_0$ is the time for which the synchronization error system (15) achieves the desired trajectory ($e = 0$); $W \geq 0$ and $U > 0$ are the suitable positive constants.

The robust feedback coupling is designed as follows:

$$u(e_1) = -\eta - U^{-1}N^{-1}(\theta(e_1))e_1,$$
$$\text{with } \theta(e_1) = T - t. \quad (19)$$

In Eq. (19), $N(t) \in \mathbb{R}$ is a continuous strictly positive function, solution of the differential Riccati equation:

$$\dot{N} = U^{-1} - WN^2. \quad (20)$$

Now, for $T > 0$ and $e_1 \in \mathbb{R}$, let us introduce the following functions which will be useful in the sequel to show that the synchronization occurs at a finite time:

$$\nu(T, e_1) = k^2 T + (N^{-1}(T))e_1^2 \quad (21)$$

$$\upsilon(T, e_1) = \nu'_T(T, e_1),$$
$$= k^2 - (U^{-1}N^{-2}(T) - W)e_1^2. \quad (22)$$

We point out that at each $e_1 \in \mathbb{R}\backslash\{0\}$, the function $\nu(T, e_1)$ achieves its minimum. Indeed, the function $\nu(T, e_1)$ is continuous (moreover, this function is analytic on $(0, \infty) \times \mathbb{R}$). Since $\|N(T)\|^{-1} \times \|e_1\| < (N^{-1}(T))e_1^2$ and $\lim_{T \to +0} \|N(T)\| = 0$, it follows that $\lim_{T \to +0} \nu(T, e_1) = +\infty$. On the other hand, one has that $\lim_{T \to +\infty} \nu(T, e_1) = +\infty$ so that the statement is verified.

We refer to the function that is defined for $e_1 \neq 0$ by equality of Eq. (19) and defined for $e_1 = 0$ by Eq. (19) with $\theta(0) = 0$ as the controllability function. At each $e_1 \neq 0$, the value of this function coincides with the minimal positive root of the equation $\upsilon(\theta, e_1) = 0$, at which the function $\nu(\theta, e_1)$ attains its global minimum (see [Korobov *et al.*, 1993]). Then, the synchronization time T is given by expression of $\theta(e_1(0))$ which is obtained by the simple resolution of equation $\upsilon(\theta, e_1) = 0$.

Now, we give some interesting properties of the controllability function $\theta(e_1)$ (see [Korobov *et al.*, 1993]).

Property 1. *From $\theta(e_1) \to 0$, it follows that $e_1 \to 0$.*

In fact,

$$\|N(\theta(e_1))\|^{-1}\|e_1\|^2 \leq \nu(\theta(e_1), e_1)$$
$$= k^2\theta + (N^{-1}(\theta(e_1))e_1^2). \quad (23)$$

On the other hand,

$$\nu(\theta, e_1) \leq \nu(1, e_1) = k^2 + (N^{-1}(1)e_1^2)$$
$$\leq k^2 + \|N^{-1}(1)\|\|e_1\|^2. \quad (24)$$

From Eqs. (23) and (24), one has

$$\|e_1\|^2(\|N(\theta(e_1))\|^{-1} - \|N^{-1}(1)\|) \leq k^2. \quad (25)$$

Let ϵ be any positive number such that

$$1 - \|N^{-1}(1)\|\epsilon > 0. \quad (26)$$

Choose $r > 0$ such that, if $0 < \theta(e_1) < r$, then $\|N(\theta(e_1))\| < \epsilon$; that is, $\|N(\theta(e_1))\|^{-1} > 1/\epsilon$. Then, when $0 < \theta(e_1) < r$, using Eqs. (25) and (26), the following inequalities

$$\|e_1\|^2 \left(\frac{1}{\epsilon} - \|N^{-1}(1)\|\right) \leq k^2 \quad \text{and}$$

$$\|e_1\|^2 \leq \frac{\epsilon k^2}{1 - \|N^{-1}(1)\|\epsilon} \quad (27)$$

are fulfilled. Hence, Property 1 is obtained.

Property 2. *When $\theta(e_1) \to 0$, then $\nu(\theta(e_1), e_1) \to 0$.*

Let ϵ be any positive number and choose $\epsilon > r > 0$ so small that when $\theta(e_1) < r$, $(N^{-1}(\epsilon)e_1^2) < \epsilon$ (this is possible because of first statement). Then $\nu(\theta(e_1), e_1) \leq \nu(\epsilon, e_1) = (k^2 + 1)\epsilon$, which proves the second statement.

Property 3. *For any initial condition $e_1(0) \in \mathbb{R}$, the solution $e_1(t)$ of (17) exists and is unique on the interval $[0, \theta(e_1(0))]$, and $\dot{\theta}(e_1(t)) = -1$ for every $t \in [0, \theta(e_1(0))]$.*

The proof of Property 3 can be found in [Korobov *et al.*, 1993].
We have the following result.

Proposition 1. *Let $\theta(e_1)$ be the controllability function, under the feedback coupling (19), the synchronization error $e_1(t)$ converges asymptotically to zero at an established finite time $T = \theta(e_1(0))$. Moreover, the closed loop performs a value of the functional (18), $J(e_1, u) = k^2\theta(e_1(0)) + N^{-1}\theta(e_1(0))e_1^2(0)$.*

Proof. Since we have $\dot{\theta}(e_1(t)) = -1$, the fact that $\lim_{t \to \theta(e_1(0))} e_1(t) \to 0$ follows from

$$\lim_{t \to \theta(e_1(0))} \theta(e_1) = \lim_{t \to \theta(e_1(0))} (\theta(e_1(0)) - t) = 0. \quad (28)$$

Let ϵ be any positive number. Consider the value of the cost functional (18) at the control $u(e_1)$ and the solution $e_1(t)$ corresponding to it, we have

$$
\begin{aligned}
J(u(e_1)) &= \lim_{\epsilon \to +0} \int_{t_0}^{\theta(e_1(0)) - \epsilon} [(Uu(e_1(t)), u(e_1(t))) \\
&\quad + (We_1(t), e_1(t))]dt + k^2\theta(e_1(0)) \\
&= \lim_{\epsilon \to +0} \int_{t_0}^{\theta(e_1(0)) - \epsilon} -\dot{\nu}(\theta(e_1(t)), e_1(t))dt \\
&= -\lim_{\epsilon \to +0} \nu(\theta(e_1(\theta(e_1(0)) - \epsilon)), \\
&\quad e_1(\theta(e_1(0)) - \epsilon)) \\
&\quad + \nu(\theta(e_1(0)), e_1(0)), \quad \text{with } t_0 = 0 \\
&= \nu(\theta(e_1(0)), e_1(0)) \\
&= k^2\theta(e_1(0)) + N^{-1}\theta(e_1(0))e_1^2(0) \\
&= \min_{\theta > 0}[k^2\theta + N^{-1}(\theta)e_1^2(0)].
\end{aligned}
$$
$$(29)$$

This completes the proof. ∎

Nevertheless, the linearizing-like feedback (19) is not physically realizable because it requires measurements of the state e_1 and a perfect knowledge of the nonlinear term η. Because the linearizing-like feedback (19) must be modified in such a way as to encompass consideration of modeling errors and parameter perturbations. We therefore use the estimation of e_1 and η in such a way that the main characteristics of the linearizing-like feedback (19) are retained. An important advantage of system (17) is that the dynamics of the state e_1 and the uncertain state η can be reconstructed from the output $y_e = e_1$.

As it has been established in [Bowong, 2004; Femat *et al.*, 1999; Gonzalez *et al.*, 1999; Kountchou *et al.*, 2014], the problem of estimating η can be addressed using a high-gain observer. Thus, the dynamics of the state η can be reconstructed from measurements of the output e_1 in the following way:

$$
\begin{cases}
\dot{\hat{e}}_1 = \hat{\eta} + u + 2L(e_1 - \hat{e}_1), \\
\dot{\hat{\eta}} = L^2(e_1 - \hat{e}_1),
\end{cases}
\quad (30)
$$

where $(\hat{e}_1, \hat{\eta})$ are estimated values of (e_1, η), and $L > 0$ is the so-called high-gain parameter. It has been proved that there exists a sufficiently large value of the high-gain parameter $L > L^*$, the dynamics of the estimation error converges exponentially to zero, see for instance [Gauthier *et al.*, 1992]. In addition, the closed-loop system is stable [Bowong, 2004; Femat *et al.*, 1999; Gonzalez *et al.*, 1999].

By using the estimated values $(\hat{e}_1, \hat{\eta})$, the feedback coupling (19) can be written as

$$u(\hat{e}_1) = -\hat{\eta} - U^{-1}N^{-1}(\theta(\hat{e}_1))\hat{e}_1, \quad (31)$$

where the matrix N is the solution of the Riccati equation (20) and U a positive constant to be determined by the designer.

3.3. *Numerical simulations*

In this section, we present the results of numerical simulations and implementation to illustrate and validate the analytical results obtained in the previous section. The parameter values of the drive and response systems have the same values: $p_1 = 5$ and $p_2 = 4$. The initial conditions were chosen as follows: $(x_1(0), x_2(0), x_3(0)) = (0.1, 0.3, 0.09)$, $(y_1(0), y_2(0), y_3(0)) = (1.1, 0.1, 0.03)$ and $(\hat{e}_1(0), \hat{\eta}(0)) = (1, 0)$. We choose $k = 5$ and $L = 400$.

We also choose $W = 1$ and $U = 1$ and a computation of Riccati equation (20) yields

$$N(t) = \frac{e^{2t} - 1}{e^{2t} + 1}. \tag{32}$$

The functions ν and υ are given by

$$\nu(\theta, \hat{e}_1) = k^2 \theta + \frac{e^{2\theta} + 1}{e^{2\theta} - 1} \hat{e}_1^2,$$
$$\upsilon(\theta, \hat{e}_1) = k^2 - \frac{4e^{2\theta}}{(e^{2\theta} - 1)^2} \hat{e}_1^2. \tag{33}$$

Solving equation $\upsilon(\theta, \hat{e}_1) = 0$ for θ gives

$$\theta(\hat{e}_1) = \frac{1}{2} \ln \frac{2\hat{e}_1^2 + k^2 + 2\sqrt{\hat{e}_1^4 + \hat{e}_1^2 k^2}}{k^2}. \tag{34}$$

Note that the other root satisfies $(2\hat{e}_1^2 + k^2 - 2\sqrt{\hat{e}_1^4 + \hat{e}_1^2 k^2})/k^2 < 1$, and is discarded. Thus, the optimal feedback coupling is

$$u(\hat{e}_1) = -\hat{\eta} - \frac{e^{2\theta} + 1}{e^{2\theta} - 1} \hat{e}_1$$
$$= -\hat{\eta} - \frac{\hat{e}_1^2 + k^2 + \sqrt{\hat{e}_1^4 + \hat{e}_1^2 k^2}}{\hat{e}_1^2 + \sqrt{\hat{e}_1^4 + \hat{e}_1^2 k^2}} \hat{e}_1. \tag{35}$$

For $\hat{e}_1(0) = 1$, the finite horizon established from Eq. (34) is $T = \theta(\hat{e}_1(0)) = 0.198$ sec (i.e. the convergence should be attained at time $t \equiv T$).

Figure 10 presents the time evolution of the synchronization errors $e_1(t)$, $e_2(t)$ and $e_3(t)$. One can observe that the synchronization error is stabilized at the origin by the output-feedback coupling (30), (35). From Fig. 10(a), it clearly appears that a fairly good convergence of e_1 is obtained in about 0.198 sec which corresponds to the finite horizon. Also, as the synchronization error (17) is minimum phase, it is easy to see that although the

feedback coupling is acting only on the state e_1, the other synchronization errors e_2 and e_3 are also stabilized at the origin.

In comparison, one more simulation study is conducted to further verify the effectiveness of the proposed feedback coupling. As predicted by the analysis of the controllability function Eq. (34), the finite horizon $T = \theta(\hat{e}_1(0))$ is determined by the control gain k and the initial condition $\hat{e}_1(0)$. The time evolution of the synchronization error $e_1(t)$, the controllability function $\theta(\hat{e}_1)$ and the function $\nu(\theta, \hat{e}_1)$ for three different values of k ($k = 4$, $k = 5$ and $k = 6$) when $\hat{e}_1(0) = 1$ are presented in Fig. 11. A fairly good convergence of the synchronization error $e_1(t)$ is obtained respectively, in about 0.247 sec, 0.198 sec and 0.165 sec which correspond to the finite horizon [see Fig. 11(a)]. Also, numerical results of Figs. 11(b) and 11(c) confirm the Properties 1 and 2, respectively.

Figure 12 presents the time evolution of the synchronization error $e_1(t)$, the controllability function $\theta(\hat{e}_1)$ and the function $\nu(\theta, \hat{e}_1)$ for three different values of $\hat{e}_1(0)$ ($\hat{e}_1(0) = 1$, $\hat{e}_1(0) = 2$ and $\hat{e}_1(0) = 3$) when $k = 5$. It clearly appears that the convergence is obtained respectively in about 0.198 sec, 0.390 sec and 0.568 sec which also correspond to the finite horizon.

Now, we investigate the robustness of the proposed scheme with respect to parameter mismatching. The parameter values of the master system (11) are chosen as $p_1 = 5$ and $p_2 = 4$ while the parameter values of the slave system (12) were chosen to be $p_1 = 4.9$ and $p_2 = 3.992$ corresponding to 0.2% of parameter mismatches. Figures 13(a) and 13(b) present the time evolution of the synchronization errors. From Fig. 13(a), it is evident that a fairly good convergence of e_2 is obtained in about the same previous synchronization time 0.198 sec
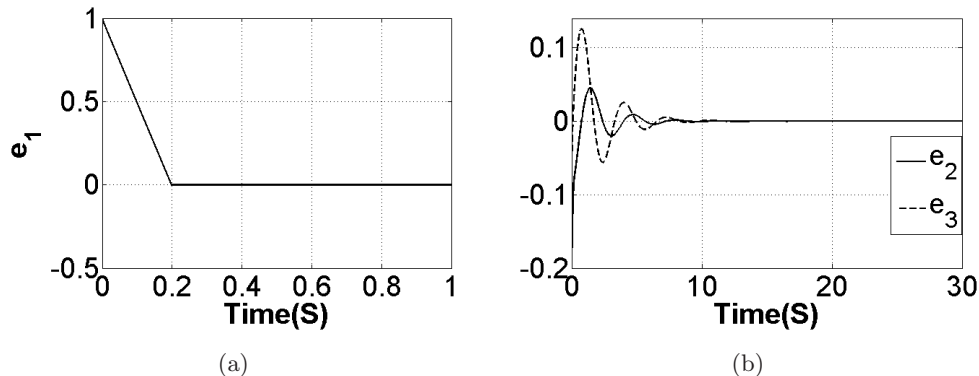

Fig. 10. Time evolution of the synchronization error. (a) $e_1 = y_1 - x_1$ and (b) $e_2 = y_2 - x_2$ and $e_3 = y_3 - x_3$.
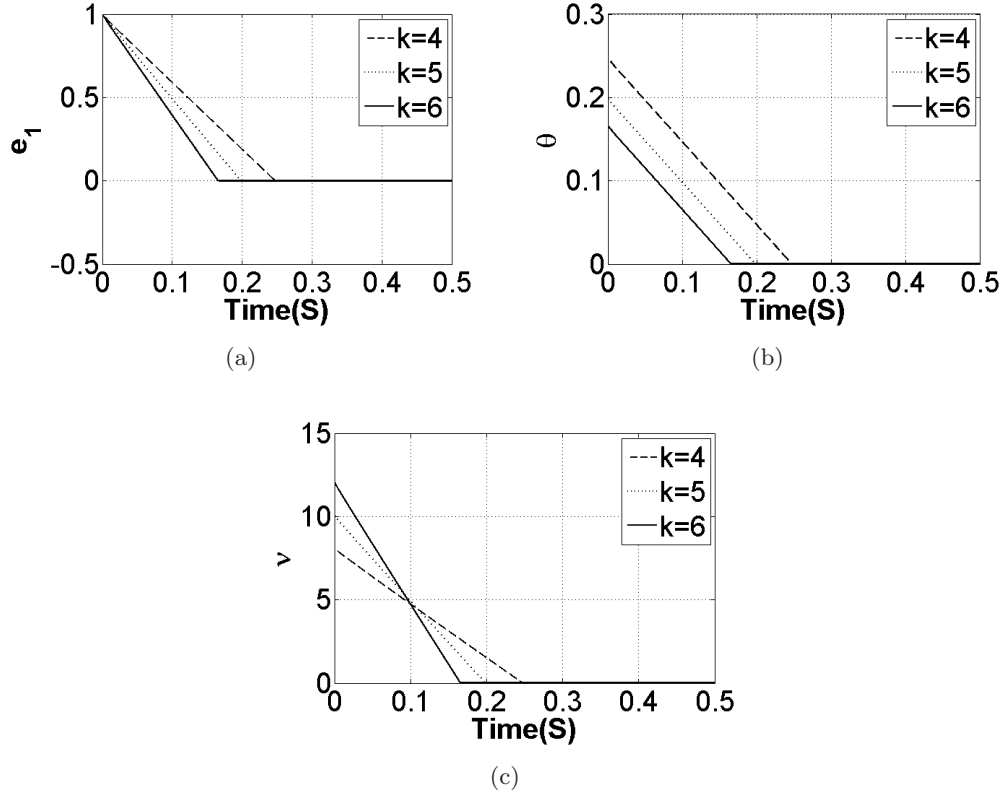
(a)

(b)

(c)

Fig. 11. Time evolution of (a) synchronization error state e_1, (b) controllability function $\theta(\hat{e}_1)$ and (c) function $\nu(\theta, \hat{e}_1)$, performed for three different values of the gain k when $\hat{e}_1(0) = e_1(0) = 1$.
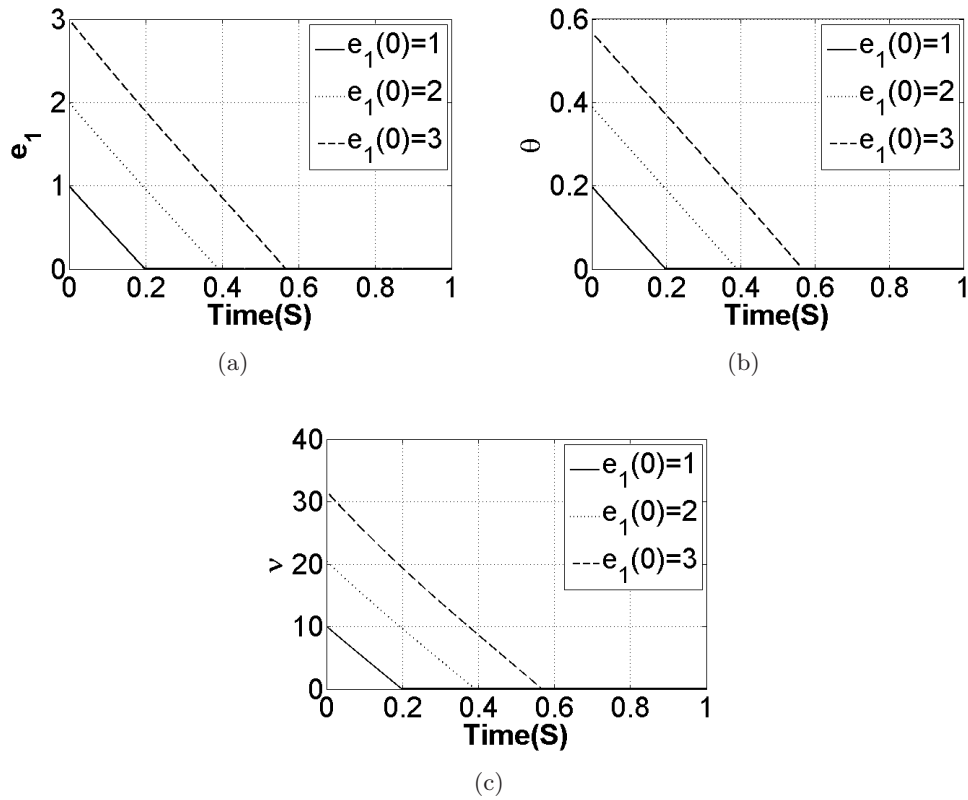

(a)

(b)

(c)

Fig. 12. Time evolution of (a) synchronization error state e_1, (b) controllability function $\theta(\hat{e}_1)$ and (c) function $\nu(\theta, \hat{e}_1)$, performed for three values of $\hat{e}_1(0) = e_1(0)$ when $k = 5$.
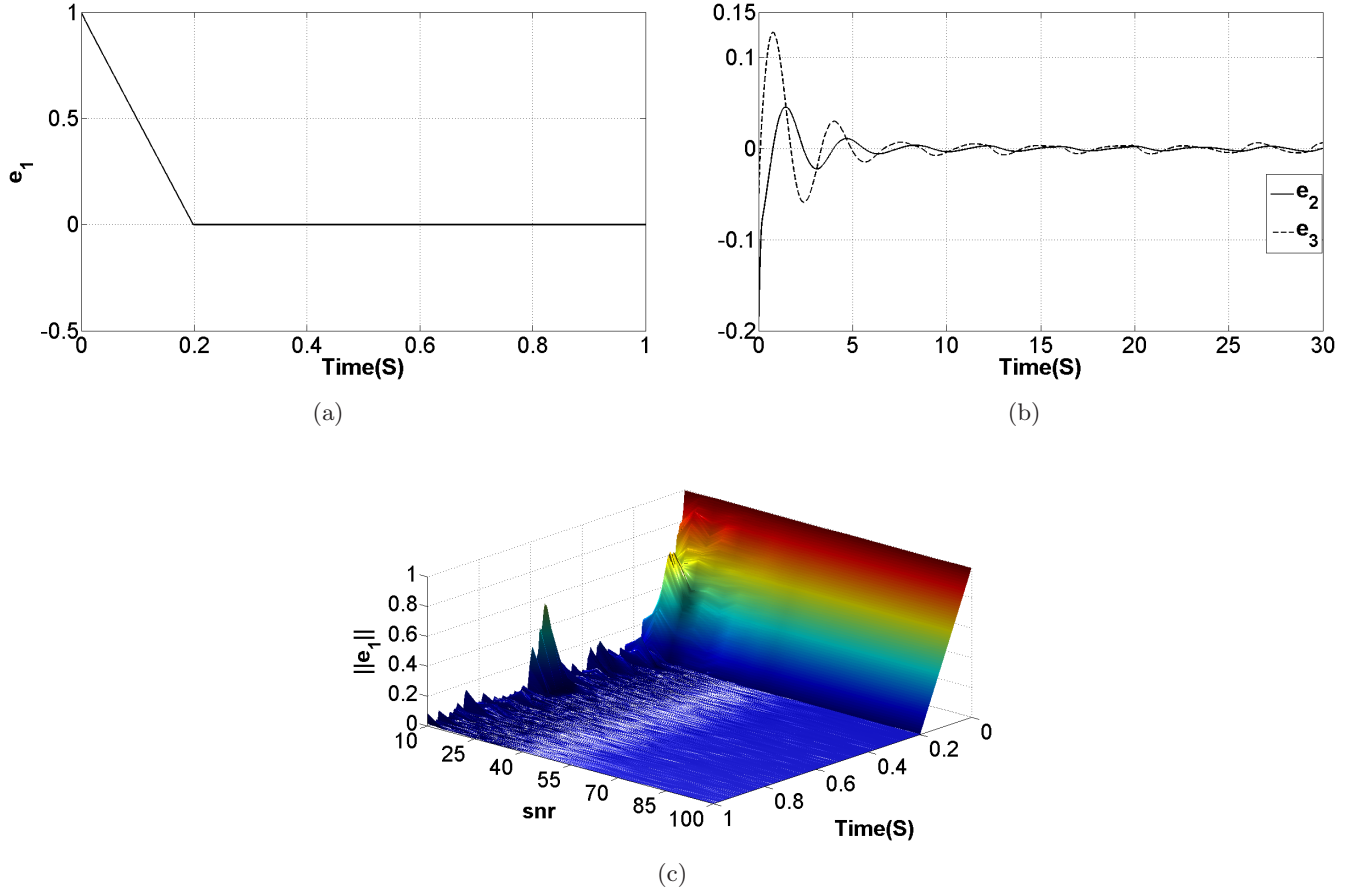
(a)

(b)

(c)

Fig. 13.   Robustness investigation of the proposed scheme in front of mismatches and noise. (a) $e_1 = y_1 - x_1$, (b) $e_2 = y_2 - x_2$ and $e_3 = y_3 - x_3$ represent the time evolution of the synchronization errors with 0.2% of parameter mismatch between the master and slave systems and (c) time evolution of error norm $\|e_1\|$ when snr is varied.

(for $k = 5$ and $\hat{e}_1(0) = 1$), which corresponds to the finite horizon in spite of the fact that both master and slave systems have different parameter values and different initial states.

Furthermore, let us investigate the robustness of the proposed scheme in front of noise. We suppose that the signal coming from the master x_1 is intrinsically modified by the channel noise and thus the channel output signal form is awgn(x_1, snr), where snr represent the signal-noise rate. As the controller is applied only on this state variable e_1, the error norm $\|e_1\|$ with numerical time and the signal-noise ratio snr is presented in Fig. 13(c). It appears from this 3D graph that, when snr increases, the synchronization is better. One can also observe that, a fairly good convergence of $\|e_1\|$ to the finite horizon 0.198 sec is obtained in spite of the presence of the noise, and of the fact that both master and slave systems have different initial states.

3.4.   *Pspice implementation*

The aim of this section is to implement a practical set-up for the synchronization strategy presented above, and to perform Pspice simulation to verify the practical feasibility of the proposed strategy. Using the values of the parameters obtained above, we determine the corresponding electronic coefficients to design and implement the electronic circuit of the synchronization scheme. The circuit diagrams of the complete master-slave-controller systems are depicted in Figs. 14–16, respectively. The values of the parameters of the feedback coupling can be obtained from the circuit component values as follows:

$$k^2 = V_k = \frac{R}{R_k}, \quad 2L = \frac{1}{10^4 R_{L1} C_{e_1}} \quad \text{and}$$
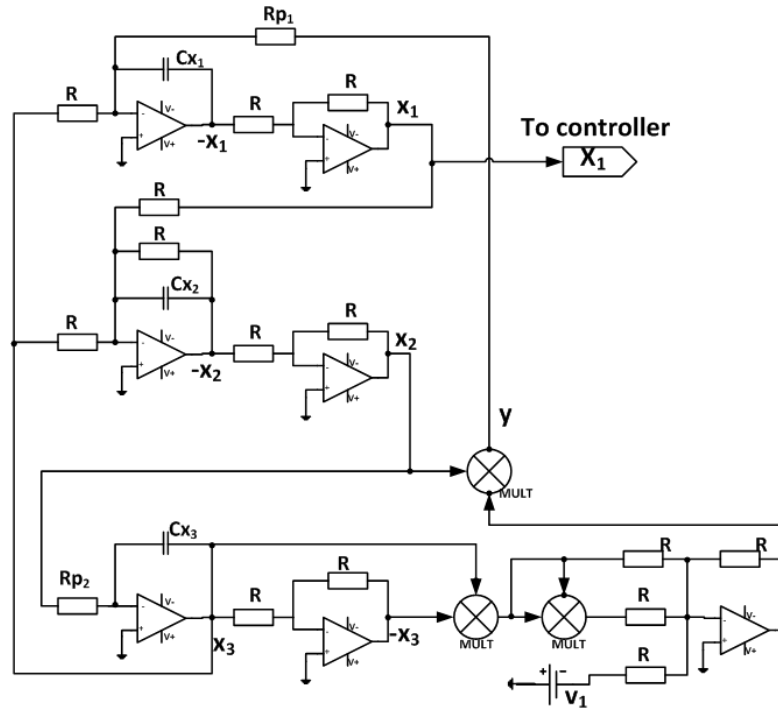
$$L^2 = \frac{1}{10^4 R_{L2} C_\eta}.$$

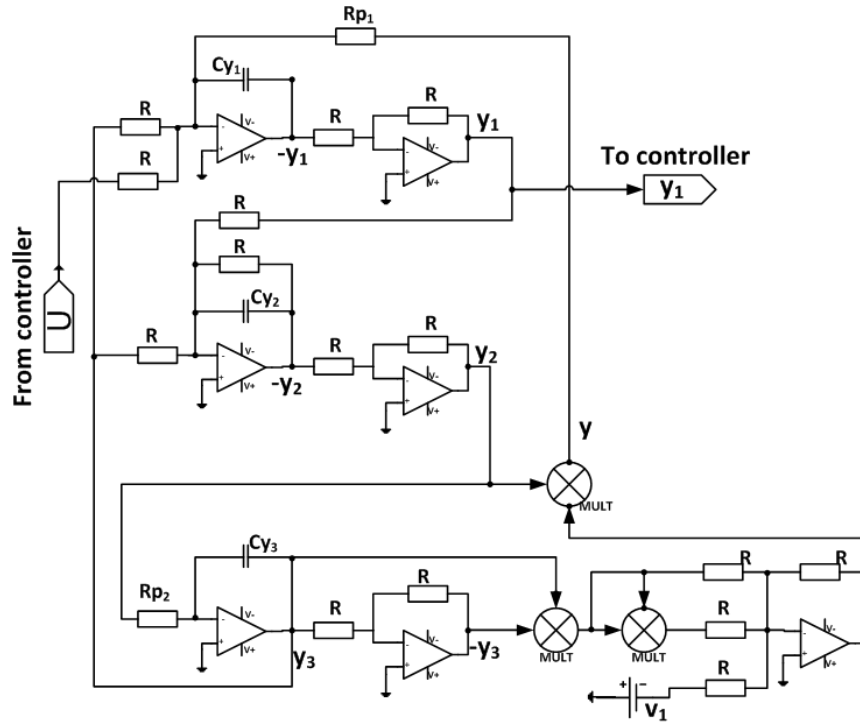Fig. 14.   Circuit diagram of the drive system (11).

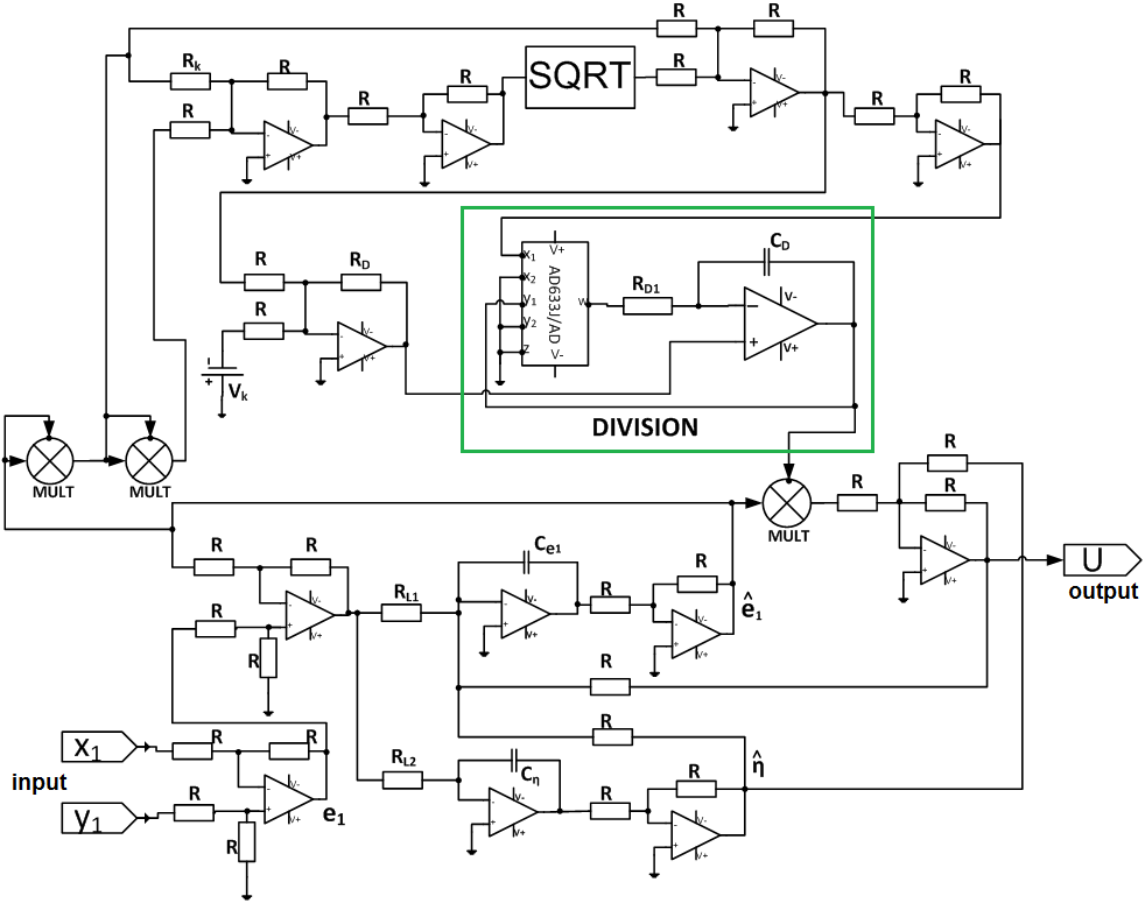Fig. 15.   Circuit diagram of the response system (12).

Fig. 16.   Circuit diagram of the feedback coupling (30) and (35).

On the feedback coupling circuit diagram of Fig. 16, the bloc 'SQRT' (which is found in the Pspice library) represents the circuit that achieves the square root while the one in green box represents the circuit that realizes the division operation for which the output voltage was the division of the inputs multiplied by 10 V.

According to the selected synchronization time of the previous section $T_M = 0.390$ sec for numerical simulations (for $k = 5$ and $\hat{e}_1(0) = 2$), the corresponding synchronization time for the Pspice simulation can be obtained as follows [see Eq. (9)]:

$$T_S = RCT_M = 39 \times 10^{-6} \text{ sec}, \tag{36}$$

where T_S and T_M are respectively, the established synchronization time through Pspice simulations and the established synchronization time using numerical simulations. We have chosen $R = 10 \text{ k}\Omega$ and $C = 10 \text{ nF}$.

Assume that the initial conditions of the master system, slave system and feedback coupling were respectively chosen to be $(V_{C_{x_1}}(0), V_{C_{x_2}}(0), V_{C_{x_3}}(0),$

$V_{C_{x_4}}(0)) = (-0.1, -0.3, -0.09)$, $(V_{C_{y_1}}(0), V_{C_{y_2}}(0),$ $V_{C_{y_3}}(0), V_{C_{y_4}}(0)) = (-2.1, -0.1, -0.03)$ and $(V_{C_D} \times$ $(0), V_{e_1}(0), V_{C_{\eta}}(0)) = (0, 2, 6)$. The circuit component values of the feedback coupling were chosen to be $C_{e_1} = C_{\eta} = C = 10 \text{ nF}$, $C_D = 22 \text{ pF}$, $R_{D1} = R = 10 \text{ k}\Omega$, $R_D = 1 \text{ k}\Omega$, $R_{L1} = 12.5 \Omega$,
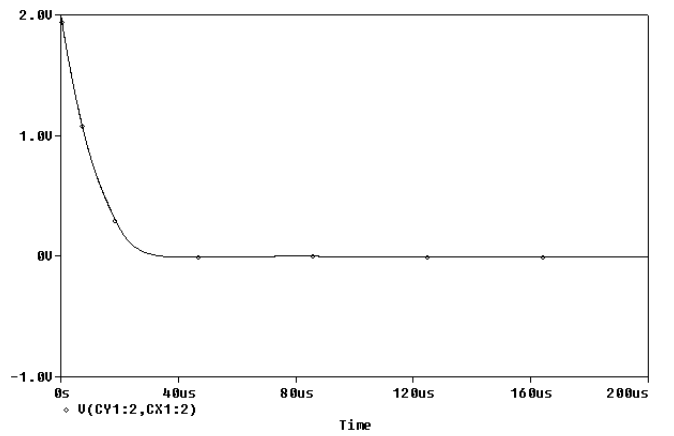

Fig. 17.   Time evolution of the synchronization error $e_1 = y_1 - x_1$ using Pspice simulations.
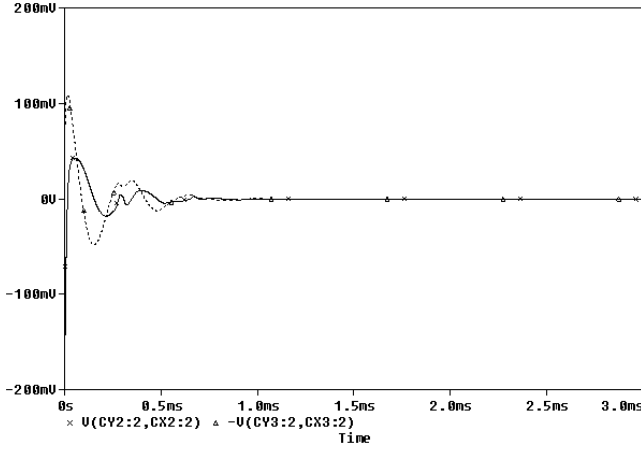
Fig. 18. Time evolution of the synchronization errors $e_2 = y_2 - x_2$ and $e_3 = y_3 - x_3$ using Pspice simulations.

$R_{L2} = 0.0625\,\Omega$, $R_k = 400\,\Omega$ and $V_k = 25\,\mathrm{V}$. The voltage source is set at $\pm 15\,\mathrm{Vdc}$. It is noted that, the effects of varying parameter k on the synchronization time (finite horizon) can be analyzed by monitoring the resistor R_k and voltage V_k while respecting the relation $k^2 = V_k = \frac{R}{R_k}$.

The Pspice simulation results of the proposed synchronization scheme are shown in Figs. 17 and 18. Note that a fairly good convergence of error e_1 is obtained in about $39\mu\,\mathrm{sec}$ which corresponds to the finite horizon. Furthermore, the synchronization errors e_2 and e_3 are also stabilized at the origin. Thus, the Pspice results confirm the practical applicability of the proposed synchronization method.

4. Conclusion

In this paper, the optimal synchronization of two identical memristive chaotic systems has been investigated. We have first studied some basic dynamical properties and chaotic behavior of a memristive system with a simple topology. An appropriate analog simulator was designed to investigate the dynamical behavior of the system. We have found a very good agreement between the results obtained using the electronic circuit and numerical simulation of the system. Later, the synchronization between two identical memristive systems was addressed. An optimal robust control scheme using the controllability functions method has been investigated. The main idea is to construct an augmented dynamical system from the synchronization error system, which is itself uncertain. Then, we have proposed a robust feedback coupling that takes into account the behavior of transient response and the feedback

coupling effort (i.e. the energy wasted by the feedback coupling action). The proposed strategy allows to set specifically the time horizon for the synchronization of two identical memristive systems. Both stability analysis and numerical simulations are presented to show the effectiveness of the optimization strategy. Also, Pspice simulations are presented to show the feasibility of the proposed synchronization scheme.

References

Adhikari, S. P., Yang, C., Kim, H. & Chua, L. O. [2012] "Memristor bridge synapse-based neural network and its learning," *IEEE Trans. Neural Netw. Learn. Syst.* **23**, 1426–1435.

Adhikari, S. P., Sah, M. P., Kim, H. & Chua, L. O. [2013] "Three fingerprints of memristor," *IEEE Trans. Circuits Syst.* **60**, 3008–3021.

Ascoli, A. & Corinto, F. [2013] "Memristor models in a chaotic neural circuit," *Int. J. Bifurcation and Chaos* **23**, 1350052-1–28.

Ascoli, A., Corinto, F., Senger, V. & Tetzlaff, R. [2013] "Memristor model comparison," *IEEE Circuits Syst. Mag.* **13**, 89–105.

Bao, B., Yu, J., Hu, F. & Liu, Z. [2014] "Generalized memristor consisting of diode bridge with first order parallel RC filter," *Int. J. Bifurcation and Chaos* **24**, 1450143-1–4.

Bowong, S. [2004] "Stability analysis for the synchronization of chaotic systems with dierent order: Application to secure communications," *Phys. Lett. A* **326**, 102–113.

Bowong, S. & Moukam-Kakmeni, F. M. [2004] "Synchronization of uncertain chaotic systems via backstepping approach," *Chaos Solit. Fract.* **21**, 999–1011.

Chua, L. O. [1971] "Memristor — The missing circuit element," *IEEE Trans. Circuit Th.* **CT-18**, 507–519.

Chua, L. O. & Kang, S. M. [1976] "Memristive devices and systems," *Proc. IEEE* **64**, 209–223.

Corinto, F., Ascoli, A. & Gilli, M. [2012] "Analysis of current-voltage characteristics for memristive elements in pattern recognition systems," *Int. J. Circuit Th. Appl.* **40**, 1277–1320.

Driscoll, T., Quinn, J., Klein, S., Kim, H. T., Kim, B. J., Pershin, Y. V., Di Ventra, M. & Basov, D. N. [2010]

"Memristive adaptive filters," *Appl. Phys. Lett.* **97**, ID093502.

Effa, J. Y., Essimbi, B. Z. & Mucho-Ngudam, J. [2009] "Synchronization of improved chaotic Colpitts oscillators using nonlinear feedback control," *Nonlin. Dyn.* **58**, 39–47.

Femat, R., Alvarez-Ramirez, J., Castillo-Toledo, B. & Gonzalez, J. [1999] "On robust chaos suppression of nonlinear oscillators: Application to Chuas circuit," *IEEE Trans. Circuits Syst.-I* **46**, 1150–1152.

Fotsin, H. B. & Daafouz, J. [2005] "Adaptive synchronization of uncertain chaotic Colpitts oscillators based on parameter identification," *Phys. Lett. A* **339**, 304–315.

Gauthier, J. P., Hammouri, H. & Othman, S. [1992] "A simple observer for a non-linear systema applications to bioreactors," *IEEE Trans. Autom. Contr.* **37**, 857–880.

Gonzalez, J., Femat, R., Alvarez-Ramirez, J., Aguilar, R. & Barron, M. A. [1999] "A discrete approach to the control and synchronization of a class of chaotic oscillators," *IEEE Trans. Circuits Syst.-I* **46**, 1139–1143.

Ho, M. C. & Hung, Y. C. [2002] "Synchronization of two different chaotic systems by using generalized active control," *Phys. Lett. A* **301**, 424–428.

Itoh, M., Yang, T. & Chua, L. O. [2001] "Conditions for impulsive synchronization of chaotic and hyperchaotic systems," *Int. J. Bifurcation and Chaos* **11**, 551–560.

Itoh, M. & Chua, L. O. [2008] "Memristor oscillators," *Int. J. Bifurcation and Chaos* **18**, 3183–3206.

Junge, L. & Parlitz, U. [2000] "Phase synchronization of coupled Ginzburg–Landau equations, " *Phys. Rev. E* **62**, 438–441.

Korobov, V. I., Krutin, V. I. & Sklyar, G. M. [1993] "An optimal control problem with a mixed cost function," *SIAM J. Contr. Optim.* **31**, 624–645.

Kountchou, M., Louodop, P., Bowong, S. & Fotsin, H. [2014] "Optimization of the synchronization of the modified Duffing system," *J. Adv. Res. Dyn. Contr. Syst.* **6**, 25–48.

Li, C. [2012] "Tracking control and generalized projective synchronization of a class of hyperchaotic system with unknown parameter and disturbance," *Commun. Nonlin. Sci. Numer. Simulat.* **17**, 405–413.

Li, J., Li, W. & Li, Q. [2012] "Sliding mode control for uncertain chaotic systems with input nonlinearity," *Commun. Nonlin. Sci. Numer. Simulat.* **17**, 341–348.

Louodop, P., Fotsin, H., Bowong, S. & Kammogne, T. S. A. [2014a] "Adaptive time-delay synchronization of chaotic systems with uncertainties using a nonlinear feedback coupling," *J. Vibr. Contr.* **20**, 815–826.

Louodop, P., Kountchou, M., Fotsin, H. & Bowong, S. [2014b] "Practical finite-time synchronization of jerk systems: Theory and experiment," *Nonlin. Dyn.* **78**, 597–607.

Lu, L., Li, C., Zhao, Z., Bao, B. & Xu, Q. [2015] "Colpitts chaotic oscillator coupling with a generalized memristor," *Math. Probl. Engin.* **2015**, 1–9.

Mahmoud, G. M. & Mahmoud, E. E. [2010] "Complete synchronization of chaotic complex nonlinear systems with uncertain parameters," *Nonlin. Dyn.* **62**, 875–882.

Muthuswamy, B. [2010] "Implementing memristor based chaotic circuits," *Int. J. Bifurcation and Chaos* **20**, 1335–1350.

Muthuswamy, B. & Chua, L. O. [2010] "Simplest chaotic circuit," *Int. J. Bifurcation and Chaos* **20**, 1567–1580.

Pecora, L. M. & Carroll, T. L. [1990] "Synchronization in chaotic systems," *Phys. Rev. Lett.* **64**, 821–824.

Pershin, Y. V. & Di Ventra, M. [2010] "Experimental demonstration of associative memory with memristive neural networks," *Neural Netw.* **23**, 881–886.

Shahverdiev, E. M., Sivaprakasam, S. & Shore, K. A. [2002] "Lag synchronization in time-delayed systems," *Phys. Lett. A* **292**, 320–324.

Shin, S., Kim, K. & Kang, S. M. [2011] "Memristor applications for programmable analog ICs," *IEEE Trans. Nanotechnol.* **10**, 266–274.

Strukov, D. B., Snider, G. S., Stewart, D. R. & Williams, R. S. [2008] "The missing memristor found," *Nature* **453**, 80–83.

Tetzlaff, R. [2014] *Memristors and Memristive Systems* (Springer, NY, USA).

Wang, L. X. [1993] "Stable adaptive fuzzy control of nonlinear systems," *IEEE Trans. Fuzzy Syst.* **1**, 146–155.

Wang, Y. W. & Guan, Z. H. [2006] "Generalized synchronization of continuous chaotic systems," *Chaos Solit. Fract.* **27**, 97–101.

Wen, S., Huang, T., Zeng, Z., Chen, Y. & Li, P. [2015] "Circuit design and exponential stabilization of memristive neural networks," *Neural Netw.* **63**, 48–56.

Yang, J. J., Strukov, D. B. & Stewart, D. R. [2013] "Memristive devices for computing," *Nat. Nanotechnol.* **8**, 13–24.

Yin, X. H., Ren, Y. & Shan, X. M. [2002] "Synchronization of discrete spatiotemporal chaos by using variable structure control," *Chaos Solit. Fract.* **14**, 1077–1082.

Zhao, H., Li, L., Peng, H., Kurths, J., Xiao, J. & Yang, Y. [2015] "Anti-synchronization for stochastic memristor-based neural networks with non-modeled dynamics via adaptive control approach," *Eur. Phys. J. B* **88**, 1–10.